

# Role of Fe(III), Phosphate, Dissolved Organic Matter, and Nitrate during the Photodegradation of Domoic Acid in the Marine Environment

JUSTINA M. FISHER,<sup>†</sup> JAMES G. REESE,<sup>†</sup>  
PERRY J. PELLECHIA,<sup>†</sup>  
PETER L. MOELLER,<sup>‡</sup> AND  
JOHN L. FERRY\*,<sup>†</sup>

Department of Chemistry and Biochemistry, University of South Carolina, Columbia, South Carolina 29208, and Coastal Center for Environmental Health and Biochemical Research, Charleston, South Carolina 29412

The photodegradation of domoic acid in model seawater containing varying amounts of total Fe(III) (expressed as Fe(III)),  $\text{NO}_3^-$ , total phosphate (expressed as  $\text{PO}_4^{3-}$ ), and dissolved organic matter (DOM) is reported. A multivariate, microscale, high-throughput experimental approach is described for evaluating how these components interact to control the removal of domoic acid from natural waters. Under the nominal conditions of the study ( $[\text{Fe(III)}]_0$  0–4  $\mu\text{M}$ ;  $[\text{NO}_3^-]_0$  0–35  $\mu\text{M}$ ;  $[\text{PO}_4^{3-}]_0$  0–4  $\mu\text{M}$ ;  $[\text{DOM}]_0$  0–10 mg/L), it is apparent that Fe(III) and DOM are significant promoters of domoic acid photooxidation. In contrast,  $\text{PO}_4^{3-}$  interacts with Fe(III) to inhibit the photooxidation of domoic acid, but  $\text{PO}_4^{3-}$  alone does not act to slow or accelerate domoic acid photodegradation. No other variables (singly or interactively) have a statistically significant impact. At an incident light intensity of 765  $\text{W/m}^2$  and initial domoic acid concentration of 0.96  $\mu\text{M}$ , domoic acid half-lives range over 12–36 h, with half-life a function of  $[\text{Fe(III)}]$ ,  $[\text{PO}_4^{3-}]$ , and dissolved organic matter loadings. An NMR based technique for measuring domoic acid–Fe(III) binding ( $1.72 \times 10^{11}$ ) is reported.

## Introduction

During harmful algal bloom events, toxins are dispersed into the food web through planktonic, detrital, or solution pathways. The diatom *Pseudo-nitzschia* in particular is known for the production of domoic acid, a tricarboxylic amino acid with neurotoxic properties (Figure 1).

This material has been linked to fish kills, poisoning of marine mammals, and human poisoning through ingestion of contaminated shellfish and finfish (1–4). Prediction of when *Pseudo-nitzschia* blooms will occur is still difficult, however there is a positive correlation between bloom events and elevated levels of the nutrients Fe(III),  $\text{PO}_4^{3-}$ , and  $\text{NO}_3^-$  (2, 5–11).

The role of Fe(III) and  $\text{NO}_3^-$  in promoting *Pseudo-nitzschia* blooms is particularly compelling because of their known photoreactivity in surface waters. Many Fe(III) complexes are known to undergo photoinduced ligand to metal charge

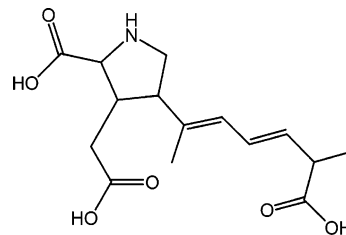


FIGURE 1. Structure of domoic acid.

transfer, and the corresponding photochemical decarboxylation of carboxylic acids is well documented (12). The reoxidation of resultant Fe(II) is rapid in seawater, allowing the system to act as a catalytic oxidant (13–16). A recent report of the photochemical instability of domoic acid solutions in the presence of Fe(III) salts suggests that this nutrient may play a more complex role in harmful algal blooms than simply promoting algal growth (17). Similarly, the photolysis of  $\text{NO}_3^-$  to produce  $\text{NO}_2^-$  and  $\text{HO}^\bullet$  is well-known (13, 18–20), and the reaction between most organics and  $\text{HO}^\bullet$  occurs with rate constants that are essentially diffusion controlled (13, 21, 22). The implication is that these two nutrients may act to promote the biological production of toxic materials in the environment while also being involved in their removal. Elevated  $\text{PO}_4^{3-}$  levels have been positively correlated with harmful algal blooms, but this ion is not photochemically active in solar UV or visible radiation (2, 5–11). However, it is possible for  $\text{PO}_4^{3-}$  to affect photochemical processes indirectly by removal of Fe(III) through the formation of insoluble or unreactive complexes (23, 24). DOM is not a nutrient, and has not been linked positively to harmful algal blooms. However, it is a ubiquitous component of surface waters that is photochemically active. It has been documented to produce oxidants such as  $\text{HO}^\bullet$ ,  $\text{HOO/O}_2^-$ , and  $^1\text{O}_2$ , etc., any of which could also potentially mitigate the effect of a harmful algal bloom by removing domoic acid from the water column (13, 19, 20, 25–30).

All four of these factors ( $\text{NO}_3^-$ , Fe(III), DOM, and  $\text{PO}_4^{3-}$ ) coexist in natural waters during any given harmful algal bloom. Since all of them are potential participants (directly or indirectly) in the domoic acid phototransformation process, a realistic model system needs to incorporate them all in such a manner that their direct impact and possible interactions can be quantified. This work reports the development of a model system based on the central composite experimental design that indexes the rate of domoic acid photodegradation against the direct impact of each factor and all possible squared factor and interfactor contributions. The central composite approach was chosen because it is particularly well-suited for detecting possible interfactor contributions with high resolution across factor levels while minimizing the total number of conditions (31, 32). The range of levels/factor was selected based on a variety of environmental measurements, and the breadth of that range makes the model output applicable across a wide range of aquatic environments (Table 1) (10, 11, 33, 34). In addition to identifying which components of the environment may play the largest role in photodegradation, the model also highlighted which pathways should be investigated at the molecular level, i.e., the complexation chemistry of Fe(III) and domoic acid.

## Experimental Procedures

**Materials.** Barnstead E-pure water (18  $\text{M}\Omega$  cm) was used for all solutions. Instant Ocean from Aqua Systems, Inc. (for

\* Corresponding author e-mail: ferry@mail.chem.sc.edu; phone: (803)777-2646; fax: (803)777-9521.

<sup>†</sup> University of South Carolina.

<sup>‡</sup> Coastal Center for Environmental Health and Biochemical Research.

**TABLE 1. Design Points for the Four-Factor Central Composite Design Used in All Experiments**

factor (units)	factor concentration levels <sup>a</sup>				
coded factor levels	-2	-1	0	1	2
factor $x_1$ : DOM (mg/L)	0.00	2.50	5.00	7.50	10.00
factor $x_2$ : Fe(III) ( $\mu$ M)	0.00	1.00	2.00	3.00	4.00
factor $x_3$ : $\text{NO}_3^-$ ( $\mu$ M)	0.00	8.75	17.50	26.25	35.00
factor $x_4$ : total $\text{PO}_4^{3-}$ ( $\mu$ M)	0.00	1.00	2.00	3.00	4.00

<sup>a</sup> Denotes initial concentrations.

composition please see Supporting Information (SI) Table 1) was used for simulating seawater after purification by C18 silica to remove trace phthalates. Freeze-dried Suwanee River natural organic matter (1R101N) was purchased from the International Humic Substances Society (for analysis and prep data please see SI Tables 2–5). Domoic acid was obtained from EMD Biosciences, Inc. at 95% purity.  $\text{Fe}_2(\text{SO}_4)_3 \cdot 5\text{H}_2\text{O}$  (97%) was purchased from Aldrich and used as received. Sodium nitrate (99%), sodium phosphate tribasic (99%), sodium bicarbonate (99%), and benzoic acid (97%) were obtained from Fisher Scientific. 1,10-phenanthroline (99%) was used as received from Sigma. Deuterium oxide ( $\text{D}_2\text{O}$ , 99.9%), sodium deuterioxide ( $\text{D}_2\text{O}$ , 99.5%, NaOD 30% w/w in  $\text{D}_2\text{O}$ ), and deuterium chloride ( $\text{D}_2\text{O}$ , 99.5%, DCl 35% w/w in  $\text{D}_2\text{O}$ ) were obtained from Cambridge Isotope Laboratories, Inc. NMR tubes were purchased from VWR and acid-cleaned before each use. Solar simulation was performed using a Suntest XLS Solar Simulator manufactured by Atlas Material Testing Solutions. Irradiation was achieved with the use of a 2200 W Xe vapor lamp, image broken by a diffuser, irradiating a 922.5  $\text{cm}^2$  polished stainless steel surface. Light intensity was set to 765  $\text{W}/\text{m}^2$  (300–800 nm) with an RSD of 7.0% with a 4.0  $\text{cm}^2$  resolution. Screw-top borosilicate vials (2 mL), purchased from Laboratory Supply Distributors, served as photoreactors.

**Experimental Design.** A 4-factor central composite design with 5 concentration levels and 6 replicates of the center point was used for this multivariate experimental design (Table 1) (32, 35, 36).

All experiments were conducted at 32 ppt salinity (Instant Ocean; SI Table 1) with an initial domoic acid concentration of 0.96  $\mu\text{M}$ . The design layout and data analysis were performed using Design Expert (version 5.0.3, Stat-Ease Inc., Minneapolis, MN). This generated 78 experiments which were then randomized.

**Photodegradation Studies.** Two 14.0  $\text{cm} \times 27.0$   $\text{cm}$  steel trays were used to hold the photoreactors. Each tray was designed to accommodate 92 photoreactors, for continuous irradiation of 184 reactors at a given time. Reactors were distributed randomly in each tray to avoid spatial bias from irregularities in the light field. All experiments were performed at a light intensity of 765  $\text{W}/\text{m}^2$  over a sample irradiation time of 15 h. Sample chamber temperature was controlled by an Atlas Suncool unit. Black standard temperature was 25–27  $^\circ\text{C}$  with chamber air temperature kept at  $21 \pm 2$   $^\circ\text{C}$ . Seven reactors containing actinometer solution were randomly distributed among the set of 78 samples on each tray (37). All vials were airtight and perpendicular to the light source. All samples were stored in the dark before and after irradiation.

**Sample Analysis.** Actinometric samples were analyzed using a Wallac 1420 fluorescence plate reader. Domoic acid samples were analyzed without any further sample treatment with an Agilent 1100 HPLC coupled to a Micromass-Quattro mass spectrometer equipped with an electrospray ion-spray (ESI) interface. Chromatographic separation was achieved using an Aqua Sep 5  $\mu\text{m}$  particle size, 10  $\text{cm} \times 2.1$  mm (i.d.)

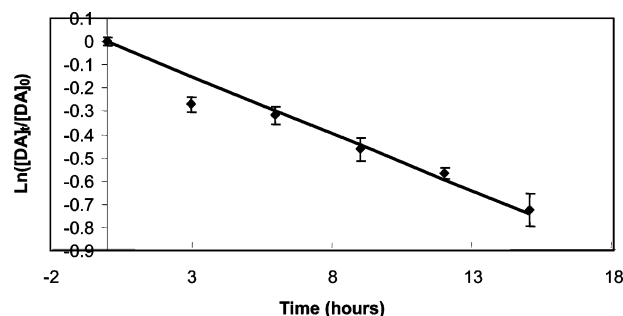


**FIGURE 2. Domoic acid rapidly photodegrades with  $t_{1/2} < 20$  h. Experimental conditions shown:  $\lambda_{\text{ex}} = 300\text{--}800$  nm; [domoic acid]<sub>0</sub> 0.96  $\mu\text{M}$  acid, 32 ppt salinity, 5 mg/L DOM, 2  $\mu\text{M}$  Fe(III), 35  $\mu\text{M}$   $\text{NO}_3^-$ , and 2  $\mu\text{M}$   $\text{PO}_4^{3-}$ .**

column (ES Industries, West Berlin, NJ) in conjunction with a corresponding Aqua Sep 5  $\mu\text{m}$  particle size, 1  $\text{cm} \times 3.2$  mm (i.d.) guard column. The LC-MS/MS procedure was as follows. A mixture of 0.1% aqueous formic acid in DI water (A) and 0.1% formic acid in acetonitrile (B) was used as the mobile phase. The initial condition was 95:5 A/B for 3 min, followed by a linear gradient over 13 min ending at 5:95 A/B. The ratio of A and B was reset to the initial condition over the following 8 min to re-establish initial conditions. The flow rate was 200  $\mu\text{L}/\text{minute}$  with a sample injection volume of 50  $\mu\text{L}$ . A 6 min solvent diversion was used to avoid salt contamination of the ion source. The MS operating conditions were set to a cone voltage of 30 V, a collision voltage of 16 eV, a source block temperature of 100  $^\circ\text{C}$ , and a desolvation temperature of 350  $^\circ\text{C}$ . The mass spectrometer was run in multiple reaction monitoring mode (MRM) with a dwell time of 0.20 s. Domoic acid was identified and quantified by analysis of the signal from the parent mass (312.36 Da) and two daughter masses (266.10 and 161.3 Da).

**$^1\text{H}$  NMR Spectroscopy.** Domoic acid solutions (642  $\mu\text{M}$ ) were prepared and spiked with  $\text{Fe}_2(\text{SO}_4)_3$  to yield a 1:1 domoic acid/Fe molar ratio. The pD was adjusted to 1.5 by the addition of 17.5% w/w DCl. NMR spectra were collected at pD increments of 0.2 ranging from 1.5 to 5.9. Additional spectra were collected at pD values of 6.15, 7.00, and 10.40. Domoic acid solution was quantitatively transferred from the NMR tube to a 5 mL conical-bottom vial between acquisitions and pD was adjusted by the addition of concentrated NaOD while stirring. The solution was returned to the NMR tube and the spectrum was collected. This process was repeated for each measurement. Proton NMR (500.211 MHz) spectra were collected on a Varian Inova 500 spectrometer with a 2.621 s acquisition time, 128 scans, 1 s recycle time, and a pulse width of 45  $^\circ$  4.2  $\mu\text{s}$ . Line width acquisition was obtained from unweighted transformed spectra utilizing the standard deconvolution routine found in VNMR 6.1c software. Presaturation was used to suppress the dominant resonance of the residual water signal. Chemical shift referencing was done by assigning a nominal value of 4.6 ppm to the residual water signal. All spectra were collected at 25  $^\circ\text{C}$  at a digital resolution of 0.38 Hz. Due to possible binding of internal chemical shift standards with Fe(III), chemical shifts reported herein and shown in figures are approximate.

## Results and Discussion

**Multivariate Photolysis Study: Kinetics of Domoic Acid Loss.** Domoic acid photodegraded upon irradiation (SI Figures 1–78), while dark control samples (SI Figure 84) showed no degradation over the time period of the experiment. This photodegradation proceeded rapidly under all experimental conditions (Figure 2), and the loss was apparently first order in domoic acid (as indicated by analysis

**TABLE 2. Experimental Parameters and the  $k_{\text{obs}}$  for Domoic Acid Photodegradation<sup>a</sup>**

run	experimental conditions <sup>b</sup>				data summary <sup>c</sup>			
	DOM (mg/L)	Fe(III) (μM)	NO <sub>3</sub> <sup>-</sup> (μM)	PO <sub>4</sub> <sup>3-</sup> (μM)	avg $k_{\text{obs}}$ ( $\times 10^{-2}$ (hr <sup>-1</sup> ))	half-life (hr)	standard error (( $\pm$ ) $\times 10^{-3}$ )	$R^2$ <sup>d</sup>
1	5.00	0.00	17.50	2.00	1.97	35.19	0.50	0.85
2	2.50	1.00	8.75	1.00	3.19	21.73	0.80	0.80
3	2.50	1.00	8.75	3.00	3.68	18.84	2.40	0.94
4	7.50	1.00	8.75	1.00	4.21	16.46	8.00	0.97
5	7.50	1.00	8.75	3.00	5.10	13.59	0.80	0.87
6	2.50	1.00	26.25	1.00	3.61	19.20	0.90	0.94
7	2.50	1.00	26.25	3.00	2.33	29.75	1.90	0.87
8	7.50	1.00	26.25	1.00	4.56	15.20	5.20	0.96
9	7.50	1.00	26.25	3.00	5.10	13.59	5.80	0.67
10	5.00	2.00	0.00	2.00	3.90	17.77	12.60	0.95
11	0.00	2.00	17.50	2.00	2.85	24.32	0.50	0.73
12	5.00	2.00	17.50	0.00	4.35	15.93	1.20	0.90
13	5.00	2.00	17.50	2.00	4.24	16.35	3.20	0.96
14	5.00	2.00	17.50	4.00	4.54	15.27	0.70	0.91
15	10.00	2.00	17.50	2.00	5.47	12.67	0.20	0.93
16	5.00	2.00	35.00	2.00	4.96	13.97	3.20	0.94
17	2.50	3.00	8.75	1.00	4.03	17.20	0.80	0.94
18	2.50	3.00	8.75	3.00	3.23	21.46	2.60	0.99
19	7.50	3.00	8.75	1.00	5.01	13.84	1.70	0.89
20	7.50	3.00	8.75	3.00	3.95	17.55	6.60	0.94
21	2.50	3.00	26.25	1.00	3.85	18.00	2.70	0.91
22	2.50	3.00	26.25	3.00	3.59	19.31	1.10	0.88
23	7.50	3.00	26.25	1.00	5.10	13.59	0.40	0.78
24	7.50	3.00	26.25	3.00	4.90	14.15	3.30	0.88
25	5.00	4.00	17.50	2.00	4.59	15.10	4.00	0.88

<sup>a</sup> All experiments contained 0.96 μM domoic acid and 32 ppt salinity. <sup>b</sup>  $n = 3$  for all experiments except run 13 (the centerpoint condition),  $n = 6$  for run 13. <sup>c</sup> Data residuals plot in SI Figure 79. <sup>d</sup> Coefficient of determination or variation about the best fit line (obtained by least-squares analysis) for  $\ln([DA]_t/[DA]_0)$  plotted versus time (hours).

of  $\ln([DA]_t/[DA]_0)$  vs time; SI Figures 1–78, 84). Direct photolysis of domoic acid was very slow in simulated seawater (0.96 μM domoic acid with 32 ppt salinity) and did not contribute significantly to the overall photodegradation rate.

The observed rate constant ( $k_{\text{obs}}$ ) was obtained by a linear least-squares analysis of the relationship between  $[DA]_t/[DA]_0$  and time for all experimental conditions (Table 2).

The relationship between  $k_{\text{obs}}$  and the four variables was evaluated by fitting a full quadratic expression to the data (eq 1) (corresponding ANOVA for the response surface, final equations expressed in coded and actual factors, and diagnostic case statistics included as SI Tables 6–8; analysis of the residuals included as SI Figure 79), including a constant term ( $\beta_0$ ), a linear coefficient for each component ( $\beta_1, \beta_2, \beta_3, \beta_4$ ), a squared coefficient for each component ( $\beta_{11}, \beta_{22}, \beta_{33}, \beta_{44}$ ), and cross-product coefficients to test for possible interactions ( $\beta_{12}, \beta_{13}, \beta_{14}, \beta_{23}, \beta_{24}, \beta_{34}$ ):

$$k_{\text{obs}} = \beta_0 + \beta_1 x_1 + \beta_2 x_2 + \beta_3 x_3 + \beta_4 x_4 + \beta_{11} x_1^2 + \beta_{22} x_2^2 + \beta_{33} x_3^2 + \beta_{44} x_4^2 + \beta_{12} x_1 x_2 + \beta_{13} x_1 x_3 + \beta_{14} x_1 x_4 + \beta_{23} x_2 x_3 + \beta_{24} x_2 x_4 + \beta_{34} x_3 x_4 \quad (1)$$

$\beta_x$  coefficients were generated during the fitting process, using the Design Expert modeling software package (Table 3).

The contributions of DOM, Fe(III), NO<sub>3</sub><sup>-</sup>, and PO<sub>4</sub><sup>3-</sup> ( $x_1, x_2, x_3$ , and  $x_4$ , respectively) to  $k_{\text{obs}}$  were evaluated by statistical analysis of the corresponding  $\beta_x$  coefficients. The hypothesis that  $\beta_x = 0$  was tested for all components. If  $t_{\text{calc}} > t_{\text{critical}}$ , then the alternative hypothesis that  $\beta_x \neq 0$  was tentatively accepted. The only  $\beta$  values that significantly differed from zero at the 95% level of confidence were those associated with DOM, Fe(III), and the interaction between Fe(III) and PO<sub>4</sub><sup>3-</sup> ( $\beta_1, \beta_2, \beta_{24}$ ) (corresponding ANOVA for the response surface, final equations expressed in coded and actual factors, and

**TABLE 3. Parameter Estimates and Hypothesis Tests for the Parameters of the Quadratic Model Fitted to the Data<sup>a</sup>**

parameter	$\beta_x$ key	standard error		$ t_{\text{calc}} $ for $H_0$ parameter = 0	prob > $ t $
		estimate ( $\times 10^{-3}$ )	( $\pm$ ) $\times 10^{-3}$		
$\beta_0$	intercept	42.00	2.33		
$\beta_1$	DOM	6.51	0.67	9.67	<0.0001 <sup>b</sup>
$\beta_2$	Fe(III)	2.33	0.67	3.32	0.0015 <sup>b</sup>
$\beta_3$	NO <sub>3</sub> <sup>-</sup>	1.14	0.67	1.69	0.0968
$\beta_4$	PO <sub>4</sub> <sup>3-</sup>	-0.55	0.67	0.81	0.4292
$\beta_{11}$	(DOM) <sup>2</sup>	-0.37	0.79	0.47	0.6419
$\beta_{22}$	Fe(III) <sup>2</sup>	-1.42	0.79	1.80	0.0766
$\beta_{33}$	(NO <sub>3</sub> <sup>-</sup> ) <sup>2</sup>	0.31	0.79	0.40	0.6935
$\beta_{44}$	(PO <sub>4</sub> <sup>3-</sup> ) <sup>2</sup>	0.34	0.79	0.43	0.6703
$\beta_{12}$	DOM–Fe(III)	-1.15	0.82	1.40	0.1664
$\beta_{13}$	DOM–NO <sub>3</sub> <sup>-</sup>	1.32	0.82	1.59	0.1158
$\beta_{14}$	DOM–PO <sub>4</sub> <sup>3-</sup>	1.23	0.82	1.50	0.1369
$\beta_{23}$	Fe(III)–NO <sub>3</sub> <sup>-</sup>	1.16	0.82	1.41	0.1649
$\beta_{24}$	Fe(III)–PO <sub>4</sub> <sup>3-</sup>	-1.81	0.82	2.20	0.0318 <sup>b</sup>
$\beta_{34}$	NO <sub>3</sub> <sup>-</sup> –PO <sub>4</sub> <sup>3-</sup>	-0.48	0.82	0.58	0.5631

<sup>a</sup> This is for the coded factor levels from Table 1. <sup>b</sup> Tests as significant at the 95% confidence level.

diagnostic case statistics included as SI Tables 9–11; analysis of the residuals included as SI Figure 80).  $\beta_1$  and  $\beta_2$  are both positive, indicating that DOM and Fe(III) both contributed positively to or accelerated the rate of photodegradation of domoic acid. The term  $\beta_{24}$  is negative, indicating that Fe(III) and PO<sub>4</sub><sup>3-</sup> interacted to reduce the photodegradation rate by forming an iron phosphate complex (e.g., Fe(PO<sub>4</sub>)<sub>x</sub>). The model for  $k_{\text{obs}}$  can be simplified accordingly as follows:

$$k_{\text{obs}} = \beta_0 + \beta_1 x_1 + \beta_2 x_2 + \beta_{24} x_2 x_4 \quad (2)$$

The  $\beta$  values for NO<sub>3</sub><sup>-</sup> and (Fe(III))<sup>2</sup> tested as significant at the 90% level of confidence, however, their effects were nearing the threshold of noise. The concentration ranges covered by those variables in this experiment are representative of those commonly encountered in near-shore waters associated with bloom events (10, 11, 33, 34). It is important to note that this study covers a limited range of conditions (Table 1), and the results are not necessarily predictive for conditions that fall outside that range.

**Molecular Interpretation.** The experimental design employed in this study sampled a broad range of prospective environmental conditions, but its ability to probe the role of specific molecular mechanisms was limited. However, it does indicate that DOM and Fe(III) are important, *independently* operating variables in domoic acid photodegradation. DOM is known to be a source of a suite of photogenerated oxidants, including hydroxyl radical, singlet oxygen, and superoxide, etc., and can also engage in photoinitiated charge-transfer reactions (13, 15, 19, 20, 25–28, 30, 38). Hydroxyl radical is unlikely to be a serious participant in this process, because the high levels of DOM and high salinity of the system (all experiments were conducted at a salinity of 32 ppt and 0.96 μM domoic acid, ionic scavengers associated with salinity in SI Table 1) should have scavenged the majority of HO• produced (22, 27, 39). Similarly, singlet oxygen should have been scavenged preferentially by reaction with DOM, halide ions, or quenching by H<sub>2</sub>O (40–42). Superoxide is not particularly reactive with amino acids (with the exception of those that contain thiols) and is unlikely to react quickly with domoic acid under our conditions (Table 2) (43, 44). The Suwannee River DOM reference material was contaminated with 8.67 ppm Fe(III) (dry weight, by the Ferrozine indicator) (45, 46). However, the lack of a negative interaction between PO<sub>4</sub><sup>3-</sup> and DOM ( $\beta_{14}$  was not significant under our conditions) indicated this contamination did not affect domoic acid photodegradation. The design was unable to

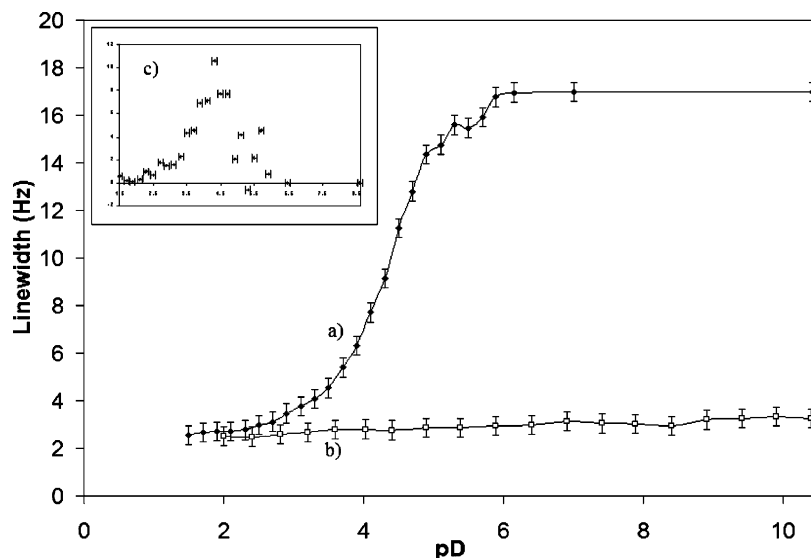


**FIGURE 3.** (a) As pD increased, the line width of the singlet at 1.8 ppm increased in the presence of Fe(III), implying the formation of a complex. [Domoic acid] = 680  $\mu\text{M}$ ; [Fe(III)] = 680  $\mu\text{M}$ ; DCl and NaOD used for pD adjustment. (b) As pD increases the line width of the singlet at 1.8 ppm remains the same for DA alone. (c) First derivative plot for inflection point assignment.

resolve the possible role of photoinduced charge transfer between DOM and domoic acid, and this remains a promising area for future investigation. Added Fe(III) directly played a significant role in domoic acid photodegradation, although the magnitude of the effect was relatively small compared to that of DOM (approximately 36%, see SI eq 1).

The role of Fe(III) in the process was probed by NMR techniques. The NMR spectrum of domoic acid (SI Figure 81) in the presence or absence of Fe(III) was obtained at varying pHs (pH 1.5–10.5). Fe(III)<sub>TOT</sub> is a paramagnetic ion that typically broadens  $^1\text{H}$  NMR peaks in aqueous samples; a through space (not through bond) effect that is a function of its proximity to the analyte (47). The  $^1\text{H}$  NMR spectrum for domoic presented a singlet at 1.8 ppm from the methyl group  $\alpha$  to the pyrrolidine ring (SI Figure 81). At low pD (1.5), line widths were the same for spectra taken with and without Fe(III), implying the domoic acid and Fe(III) were not associated (Figure 3).

As pD increased, the line widths broadened rapidly in the sample containing Fe(III), but remained essentially unchanged in the sample with domoic acid alone. Since [Fe(III)] was not high enough to cause line broadening at low pD, at higher pD line broadening must have been a consequence of complexation. Such a complex is quite likely to undergo photodegradation through ligand-to-metal photoinduced charge transfer, a process that has been thoroughly documented for other organic acids that ligate photoactive metals (17, 33, 48–52).

This behavior is consistent with that of other amino acids (e.g., EDTA) that complex metals strongly in the deprotonated form but only very weakly in acidic environments (53). The titration curve obtained from plotting line width versus pD demonstrated a single inflection point at pD 4.4, suggesting the resulting complex had a 1:1 stoichiometry. An association constant,  $K$ , for the domoic acid–Fe(III) complex was estimated based on the assumption that domoic acid, like other amino acids, complexes metals most effectively in the fully deprotonated ( $\text{Y}^{3-}$ ) form (53). Based on the position of the inflection point, known  $\text{pK}_\text{a}$ s of domoic acid (54), and the initial concentrations of Fe(III) and domoic acid, the estimated value of  $K$  was  $1.72 \times 10^{11}$ . This value is in close agreement with the measured value of  $10^{8.7 \pm 0.5}$  estimated by stripping voltammetry (33).

The photostability of this complex was tested by exposing domoic acid (0.96  $\mu\text{M}$ , initially) to simulated sunlight in the

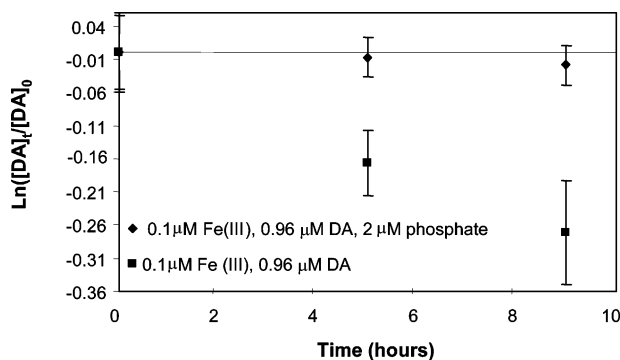


**FIGURE 4.** Domoic acid photodegrades quickly in the presence of Fe(III), but this photodegradation is greatly inhibited by the addition of  $\text{PO}_4^{3-}$ . Experimental conditions are those within the experimental matrix.

presence of Fe(III) (0.10  $\mu\text{M}$ ). In these experiments, domoic acid in solution quickly photodegraded with a rate of 0.031  $\text{hr}^{-1}$ , although in the absence of Fe(III) its direct photolysis was negligible. When the experiment was repeated in the presence of 2.00  $\mu\text{M}$   $\text{PO}_4^{3-}$ , the photodegradation of domoic acid was reduced by a factor of  $\sim 15$ , to 0.002  $\text{hr}^{-1}$  (Figure 4). The implication was that  $\text{PO}_4^{3-}$ , which associates strongly with Fe(III) ( $K \approx 10^{40}$ ) (11, 53) out competed domoic acid for Fe(III) and so eliminated the Fe–domoic acid complex photolysis pathway. This was in agreement with the negative value of  $\beta_{24}$ . In these experiments, Fe(III) and  $\text{PO}_4^{3-}$  were added prior to the addition of domoic acid, to better simulate the natural condition where domoic acid is generated in the water column.

**Product Qualification.** The small volumes used in this study, coupled with the effort to keep the reactant concentrations as environmentally relevant (and therefore low) as possible, precluded the use of large-scale preconcentration techniques in sample analysis. Accordingly, an attempt was made to qualify products using LC–MS (vide supra), but they were not quantifiable. Two peaks dominated the chromatograms of the photolyzed mixture with apparent molecular ions of 327 and 273 (mass spectra presented as SI Figures 82 and 83, respectively). These masses are consistent with the addition of an oxygen to the parent molecule from the partial oxidation of the allylic side chain to the corresponding enone (mass 327) and a decarboxylation product (mass 273) (55).

However, the lack of analytical standards for these products made their quantification impossible.

**Environmental Significance.** The growth and impact of harmful algal blooms is notoriously difficult to predict based on water quality parameters, although models are improving. The blooms themselves are capable of affecting hundreds of square miles of open water and coastal regions, with correspondingly large economic and public health impacts, and the long term environmental fate of the toxins they produce is essentially unknown. These experiments represent early, necessary efforts to evaluate how such biomolecules may be attenuated by complex photochemical processes in the environment. However, there are some important caveats. The range of each variable is high, compared to typical coastal seawaters, an approach selected to be conservative in estimating the strongest possible effect of a given factor. The DOM used in this study was from the Suwannee River, which is certainly relevant to the Southeastern United States but may be less so for other parts of the world. Nonetheless, the multifactor approach of this study provides valuable insight into how the different variables that affect bloom growth may act, alone or in concert, to moderate the eventual environmental impact of the event.

## Acknowledgments

We are very grateful to Drs. Mike Walla and Bill Cotham for all their assistance with mass spectrometry. This work was supported by the U.S. Environmental Protection Agency Grant RD83-1042.

## Supporting Information Available

Information regarding the composition of Instant Ocean, natural organic matter isolation and composition data, domoic acid degradation kinetics, and the statistical ANOVA data for the matrix. This material is available free of charge via the Internet at <http://pubs.acs.org>.

## Literature Cited

- Yasumoto, T.; Murata, M. Marine Toxins. *Chem. Rev.* **1993**, *93*, 1897–1909.
- Hallegraeff, G. M. A review of harmful algal blooms and their apparent global increase. *Phycologia* **1993**, *32*, 79–99.
- Anderson, D. M. Turning back the harmful red tide. *Nature* **1997**, *388*, 513–514.
- Mos, L. Domoic Acid: a fascinating marine toxin. *Environ. Toxicol. Pharmacol.* **2001**, *9*, 79–85.
- Wells, M. L. The level of iron enrichment required to initiate diatom blooms in HNLC waters. *Mar. Chem.* **2003**, *82*, 101–114.
- Maldonado, M. T.; Hughes, M. P.; Rue, E. L.; Wells, M. L. The effect of Fe and Cu on growth and domoic acid production by *Pseudo-nitzschia*. *Limnol. Oceanogr.* **2002**, *47*, 515–526.
- Trainer, V. L.; Adams, N. G.; Bill, B. D.; Stehr, C. M.; Wekell, J. C.; Moeller, P.; Busman, M.; Woodruff, D. Domoic Acid Production Near California Coastal Upwelling Zones, June 1998. *Limnol. Oceanogr.* **2000**, *45*, 1818–1833.
- Trainer, V. L.; Hickey, B. M.; Horner, R. A. Biological and physical dynamics of domoic acid production off the Washington coast. *Limnol. Oceanogr.* **2002**, *47*, 1438–1446.
- Marchetti, A.; Trainer, V. L.; Harrison, P. J. Environmental conditions and phytoplankton dynamics associated with *Pseudo-nitzschia* abundance and domoic acid in the Juan de Fuca eddy. *Mar. Ecol. Prog. Ser.* **2004**, *281*, 1–12.
- Bruland, K. W.; Rue, E. L.; Smith, G. J. Iron and macronutrients in California coastal upwelling regimes: Implications for diatom blooms. *Limnol. Oceanogr.* **2001**, *46*, 1661–1674.
- Hoppe, H.-G. Phosphatase activity in the sea. *Hydrobiologia* **2003**, *493*, 187–200.
- Faust, B. C.; Zepp, R. G. Photochemistry of Aqueous Iron(III)–Polycarboxylate Complexes: Roles in the Chemistry of Atmospheric and Surface Waters. *Environ. Sci. Technol.* **1993**, *27*, 2517–2522.
- Zepp, R. G.; Faust, B. C.; Hoigne, J. Hydroxyl Radical Formation in Aqueous Reactions (pH 3–8) of Iron (II) with Hydrogen Peroxide: The Photo-Fenton Reaction. *Environ. Sci. Technol.* **1992**, *26*, 313–319.
- White, E. M.; Vaughan, P. P.; Zepp, R. G. Role of the photo-Fenton reaction in the production of hydroxyl radicals and photobleaching of colored dissolved organic matter in a coastal river of the southeastern United States. *Aquat. Sci.* **2003**, *65*, 402–414.
- Haag, W. R.; Yao, C. C. D. Rate constants for reaction of hydroxyl radicals with several drinking water contaminants. *Environ. Sci. Technol.* **1992**, *26*, 1005–1013.
- Zhao, X.-K.; Yang, G.-P.; Wang, Y.-J.; Gao, X.-C. Photochemical degradation of dimethyl phthalate by Fenton reagent. *J. Photochem. Photobiol., A* **2004**, *161*, 215–220.
- Bates, S. S.; Leger, C.; Wells, M. L.; Hardy, K. In *Proceedings of the Eighth Canadian Workshop on Harmful Marine Algae*; Bates, S. S., Ed.; Fisheries and Oceans Canada: Moncton, NB, Canada, 2003; pp 30–36.
- Zafiriou, O. C.; True, M. B. Nitrate Photolysis in Seawater by Sunlight. *Mar. Chem.* **1979**, *8*, 33–42.
- Zafiriou, O. C. Sources and reactions of hydroxyl and daughter radicals in sea water. *J. Geophys. Res.* **1974**, *79*, 4491–4497.
- Zepp, R. G.; Hoigne, J.; Bader, H. Nitrate-induced photooxidation of trace organic chemicals in water. *Environ. Sci. Technol.* **1987**, *21*, 443–450.
- Kwan, W. P.; Voelker, B. M. Rates of Hydroxyl Radical Generation and Organic Compound Oxidation in Mineral-Catalyzed Fenton-like Systems. *Environ. Sci. Technol.* **2003**, *37*, 1150–1158.
- Takeda, K.; Hiroshi, T.; Yanaji, S.; Ohta, K.; Sakugawa, H. Determination of Hydroxyl Radical Photoproduction Rates in Natural Waters. *Anal. Sci.* **2004**, *20*, 153–158.
- Mauzerall, D.; Borowska, Z.; Zielinski, I. Photo and Thermal-Reactions of Ferrous Hydroxide. *Origins Life Evol. Biosphere* **1993**, *23*, 105–114.
- Perezruiz, T.; Martinezlozano, C.; Tomas, V. Photo-Oxidation of Acridine and Acridine Yellow in the Presence of Iron(III) – Determination of Micro-Amounts of Iron, Fluoride and Phosphate. *Analyst* **1984**, *109*, 1401–1404.
- Zafiriou, O. C.; True, M. B. Nitrite Photolysis in Seawater by Sunlight. *Mar. Chem.* **1979**, *8*, 9–32.
- Zepp, R. G. W.; Lee, N.; Baughman, G. L.; Hollis, R. C. Singlet oxygen in natural waters. *Nature* **1977**, *267*, 421–423.
- Haag, W. R.; Hoigne, J. Singlet oxygen in surface waters: 3. Photochemical formation and steady-state concentrations in various types of waters. *Environ. Sci. Technol.* **1986**, *20*, 341–348.
- Hessler, D. P. F.; Fritz, H.; Oliveros, E.; Braun, A. M. Quenching of singlet oxygen by humic substances. *J. Photochem. Photobiol., B* **1996**, *36*, 55–60.
- Hoigne, J. B. Heinz Ozonation of water: Kinetics of Oxidation of Ammonia by Ozone and Hydroxyl Radicals. *Environ. Sci. Technol.* **1978**, *12*, 79–84.
- Goldstone, J. V.; Pullin, M. J.; Bertilsson, S.; Voelker, B. M. Reactions of Hydroxyl Radical with Humic Substances: Bleaching, Mineralization, and Production of Bioavailable Carbon Substrates. *Environ. Sci. Technol.* **2002**, *36*, 364–372.
- NIST/SEMATECH. *e-Handbook of Statistical Methods*. <http://www.itl.nist.gov/div898/handbook/>, accessed November 15, 2005.
- Johnson, R. A.; Wichern, D. W. *Applied Multivariate Statistical Analysis*, 5th ed.; Prentice Hall: Upper Saddle River, NJ, 2002.
- Rue, E.; Bruland, K. Domoic Acid binds iron and copper: a possible role for the toxin produced by the marine diatom *Pseudo-nitzschia*. *Mar. Chem.* **2001**, *76*, 127–134.
- Otero, E.; Culp, R.; Noakes, J. E.; Hodson, R. E. The distribution and  $\delta^{13}\text{C}$  of dissolved organic carbon and its humic fraction in estuaries of southeastern USA. *Estuarine, Coastal Shelf Sci.* **2003**, *56*, 1187–1194.
- Deming, S. N.; Morgan, S. L. *Experimental Design: A Chemometric Approach*, 2nd ed.; Elsevier Science Publishers B. V.: Amsterdam, 1993.
- Montgomery, D. C. *Design and Analysis of Experiments*, 5th ed.; John Wiley & Sons: New York, 2001.
- Kieber, R. J.; Li, A.; Seaton, P. J. Production of nitrite from the photodegradation of dissolved organic matter in natural waters. *Environ. Sci. Technol.* **1999**, *33*, 993–998.
- Zhu, D.; Hyun, S.; Pignatello, J. J.; Lee, L. S. Evidence for  $\pi$ – $\pi$  electron donor–acceptor interactions between  $\pi$ -donor aromatic compounds and  $\pi$ -acceptor sites in soil organic matter through pH effects on sorption. *Environ. Sci. Technol.* **2004**, *38*, 4361–4368.

- (39) Zepp, R. G. W.; Lee, N.; Baughman, G. L.; Hollis, R. C. Singlet oxygen in natural waters. *Nature* **1977**, *267*, 421–423.
- (40) Kong, L.; Ferry, J. L. Photochemical oxidation of chrysene at the silica gel-water interface. *J. Photochem. Photobiol., A* **2004**, *162*, 415–421.
- (41) Rosenthal, I.; Frimer, A. The quenching effect of iodide ion on singlet oxygen. *Photochem. Photobiol.* **1976**, *23*, 209–211.
- (42) Braathen, G.; Chou, P. T.; Frei, H. Time-resolved reaction of O<sub>2</sub>(<sup>1</sup>Δ) with iodide in aqueous solution. *J. Phys. Chem.* **1988**, *92*, 6610–6615.
- (43) Matheson, I. B. C.; Etheridge, R. D.; Kratowich, N. R.; Lee, J. Quenching of singlet oxygen by amino acids and proteins. *Photochem. Photobiol.* **1975**, *21*, 165–171.
- (44) Michaeli, A.; Feitelson, J. Reactivity of singlet oxygen toward amino acids and peptides. *Photochem. Photobiol.* **1994**, *59*, 284–289.
- (45) Stookey, L. L. Ferrozine— A New Spectrophotometric Reagent for Iron. *Anal. Chem.* **1970**, *42*, 779–781.
- (46) Viollier, E.; Inglett, P. W.; Hunter, K.; Roychoudhury, A. N.; Van Cappellen, P. The Ferrozine method revisited: Fe(II)/Fe(III) determination in natural waters. *Appl. Geochem.* **2000**, *15*, 785–790.
- (47) Bloembergen, N.; Purcell, E. M.; Pound, R. V. Relaxation Effects in Nuclear Magnetic Resonance Absorption. *Phys. Rev.* **1948**, *73*, 679–712.
- (48) Kwan, W. P.; Voelker, B. M. Decomposition of Hydrogen Peroxide and Organic compounds in the Presence of Dissolved Iron and Ferrihydrite. *Environ. Sci. Technol.* **2002**, *36*, 1467–1476.
- (49) Macrellis, H. M.; Trick, C. G.; Rue, E. L.; Smith, G.; Bruland, K. W. Collection and detection of natural iron-binding ligands from seawater. *Mar. Chem.* **2001**, *76*, 175–187.
- (50) McArdell, C. S.; Stone, A. T.; Tian, J. Reaction of EDTA and Related Aminocarboxylate Chelating Agents with Co<sup>III</sup>OOH (Heterogenite) and Mn<sup>III</sup>OOH (Manganite). *Environ. Sci. Technol.* **1998**, *32*, 2923–2930.
- (51) Rose, A. L.; Waite, T. D. Kinetics of iron complexation by dissolved natural organic matter in coastal waters. *Mar. Chem.* **2003**, *84*, 85–103.
- (52) Strathmann, T. J.; Stone, A. T. Reduction of Oxamyl and Related Pesticides by Fe<sup>II</sup>: Influence of Organic Ligands and Natural Organic Matter. *Environ. Sci. Technol.* **2002**, *36*, 5172–5183.
- (53) Harris, D. C. *Exploring Chemical Analysis*, 2nd ed.; W. H. Freeman and Company: New York, 2001.
- (54) Walter, J. A.; Leek, D. M.; Falk, M. NMR study of the protonation of domoic acid. *Can. J. Chem.* **1992**, *70*, 1156–1161.
- (55) von Sonntag, C.; Schuchmann, H.-P. The Elucidation of Peroxyl Radical Reactions in Aqueous Solution with the Help of Radiation-Chemical Methods. *Angew. Chem., Int. Ed.* **1991**, *30*, 1229–1253.

*Received for review July 22, 2005. Revised manuscript received January 27, 2006. Accepted February 6, 2006.*

ES051443B